Discrete modeling of penetration tests in constant velocity and impact conditions

Quoc Anh Tran, Bastien Chevalier, Pierre Breul

Discrete modeling of penetration tests in constant velocity and impact conditions

Quoc Anh Tran, Bastien Chevalier and Pierre Breul

Correspondence to bastien.chevalier@univ-bpclermont.fr

Clermont Université, Université Blaise Pascal, Institut Pascal, BP 10448, F-63000 Clermont-Ferrand, France.

CNRS, UMR 6602, Institut Pascal, F-63171 Aubière, France.

Tel. +33(0)4.73.40.75.23

Fax. +33(0)4.73.40.74.94

Abstract

The paper presents investigations on the penetration tests in granular material. A discrete numerical study is proposed for the modeling of penetration tests in constant velocity conditions and also in impact conditions. The model reproduces qualitatively the mechanical response of samples of granular material, compared to classical experimental results. Penetration tests are conducted at constant velocity and from impact, with similar penetration rates ranging from 25 $mm.s^{-1}$ to 5000 $mm.s^{-1}$. In constant velocity condition, the value of tip force remains steady as long as the penetration velocity induces a quasi–static regime in the granular material. However, the tip force increases rapidly in the dense flow regime corresponding to higher penetration rate. Impact tip force increases with the impact velocity. Finally, the tip forces obtained from impact penetration tests are smaller compared to the one obtained in constant velocity conditions in both quasi–static and dense flow regimes.

Keywords: DEM, Penetration test, Tip force, Penetration rate

Computers and Geotechnics 71 (2016) 12–18

http://dx.doi.org/10.1016/j.compgeo.2015.08.010

Article history:

Received 13 February 2015

Received in revised form 18 August 2015

Accepted 31 August 2015

1. Introduction

In the field of in situ mechanical characterization of soils, penetration tests are commonly used. The tip resistances, deduced from pile driving theory, can be measured either in dynamic (q_d) (Fig.1) or in static conditions (q_c).

Recently, the measurement technique in impact conditions was improved. It is now possible to record the real–time response of the soil during one impact in terms of tip force and penetration distance [1,2] (Fig.2). Mechanical properties other than the classical tip resistance might be extracted from this new kind of experimental measurements. Recent studies from [3] and [4] showed the interest in penetration tests for the characterization of coarse material.

Penetration tests generate large deformations and a highly non-homogeneous solicitation, Discrete Element Method (DEM) is then a particularly relevant numerical method to model this test. Many authors proposed numerical models for reproducing penetration tests in static conditions i.e. in constant velocity conditions in 2D [5,6,7,8,9,10] and in 3D [1,4,11,12]. However, [1,13,14] showed that tip resistance depends on the loading type used in the penetration process. Very few researches focus to the modeling of penetration tests in impact conditions.

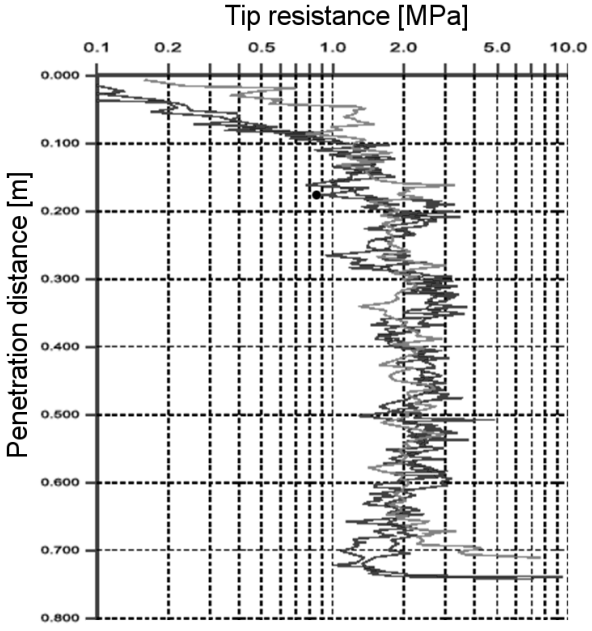

Figure 1. Example of an experimental result of a impact penetration test.

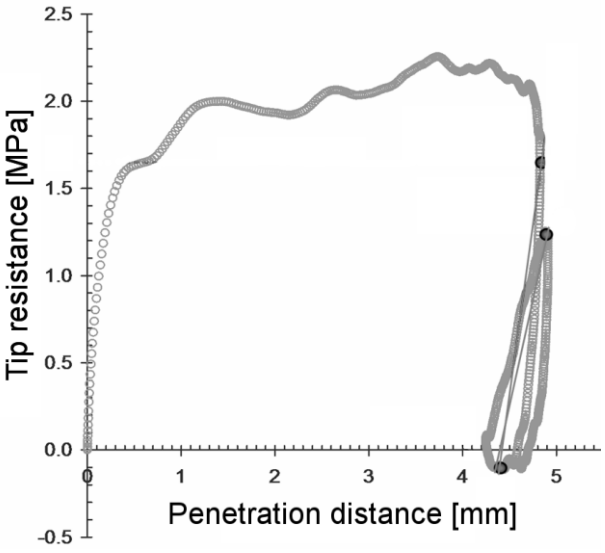

Figure 2. Example of experimental load–penetration curve obtained in a impact penetration test for one impact [2].

In this paper, we propose a numerical model of penetration tests using DEM for reproducing tests in both constant velocity and impact conditions in coarse materials. The penetration device modeled here is a light penetrometer [3,4]. Macroscopic results are discussed in this paper. After the description of the numerical model, we present the effect of penetration rate on the tip force obtained from both constant velocity and impact penetration tests will. Finally, a comparison of the tip force obtained with both loading types is proposed and discussed.

2. Numerical Model

Discrete Element Method in two dimensions was used with Itasca's software PFC^{2D} [15]. Table 1 summarize the parameter of the model. Granular material samples of 10 000 cylindrical particles were generated and tested in a rectangular box (Table 1). A diameter ratio of 2 was chosen between largest and smallest particles. The average particle diameter of the material D_p is equal to 5.4 mm (Fig.3).

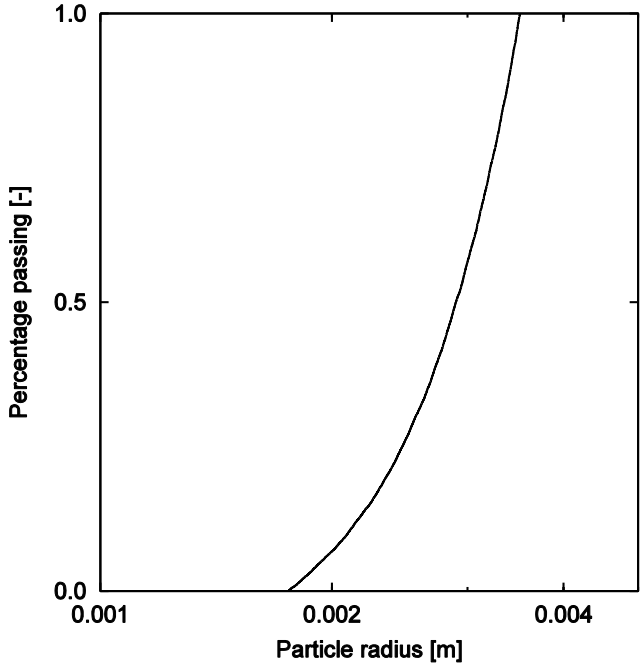

Figure 3. Particle size distribution of the granular material.

The sample preparation broke down into 3 steps. First, a frictionless particle radius expansion method without gravity was used in order to reach a minimum value of sample porosity of $n = 0.15$. Secondly, the final value of friction coefficient of $\mu_{particle} = 1.00$ was applied as well as the gravity. We conducted simulations with different values of particle friction and found no influence of particle friction on the results for values of $\mu_{particle} \geq 0.50$. So the value of $\mu_{particle} = 1.00$ was chosen. The sample was then stabilized until equilibrium state was reached.

At the end of this step, the internal stress state at center of the sample was calculated. The ratio between horizontal and vertical stresses was found equal to 0.5, which is close to classical "at rest" earth pressure ratio K_0. This ratio was also calculated from the stresses measured on sample boundaries. Finally, the sample was confined vertically on its top surface.

Usually in homogeneous soils, tip resistance first increases with depth until a critical depth is reached and then tip resistance becomes steady (Fig.1). The confining stress, equal to 40 kPa simulates an overlaying layer of material; it prevented the effects of free surface to be observed [14]. A linear contact model was used and the contact stiffness was chosen in order to assess the assumption of rigid particles during penetration tests [16,17]. A Coulomb friction criterion of coefficient $\mu_{particle} = 1.00$ was used to limit the value of tangential force relatively to normal force. No viscous damping was considered in the contact model and no local damping was used in the model [18]. Thus, energy is only dissipated by friction during the penetration tests.

Parameter	*Symbol*	*Value*	*Unit*
Width box	L	0.6	m
Height box	H	0.45	m
Particle number	N_P	10 000	–
Average particle diameter	D_p	5.4	m
Particle density	ρ	2 700	$kg.m^{-3}$
Normal contact stiffness	k_n	1.25×10^8	N/m
Tangential contact stiffness	k_s	9.375×10^7	N/m
Particle friction coefficient	$\mu_{particle}$	1.00	-
Rod friction coefficient	μ_{rod}	0.00	-
Tip friction coefficient	μ_{tip}	0.30	-

Table 1. A summary table with all DEM parameters used in penetration tests.

Penetration tests were conducted on three different samples generated with the same conditions of density and particle grading but different initial particle arrangement. The penetration was performed with a frictionless rod of width 14 mm linked to a tip of 16 mm width at its bottom edge and presenting a friction coefficient μ_{tip} of 0.3 [2,3,4] (Fig.4). In constant velocity conditions, called hereafter constant velocity conditions test, the rod is driven in the sample with a constant rod velocity up to 0.30 m of depth. The vertical

component of the force applied by the granular material on the tip is called tip force F_c for penetration test conducted in constant velocity condition.

For tests conducted in impact conditions, the rod is first driven with constant velocity until a depth of 0.15 m is reached. The rod is then released and stabilized under its own weight. Then, series of five successive impacts are produced in each sample with an additional cylinder on the top of the rod (Fig.4). The mass of the impacting cylinder is equal to the rod mass. The vertical component of the force applied by the granular material on the tip is called tip force F_d in impact condition tests. Equilibrium state is reached after each blow and before applying the next blow.

The equilibrium state used in the simulations is a classical equilibrium state condition. Once one of the two ratio values defined hereafter decreases below a given value, the system is considered in mechanical equilibrium. The first ratio is given by the ratio of average unbalanced force magnitude of particles to average magnitude of normal contact force. The second ratio is given by the ratio of the magnitude of the greatest unbalanced force on particles to the magnitude of the greatest normal contact force.

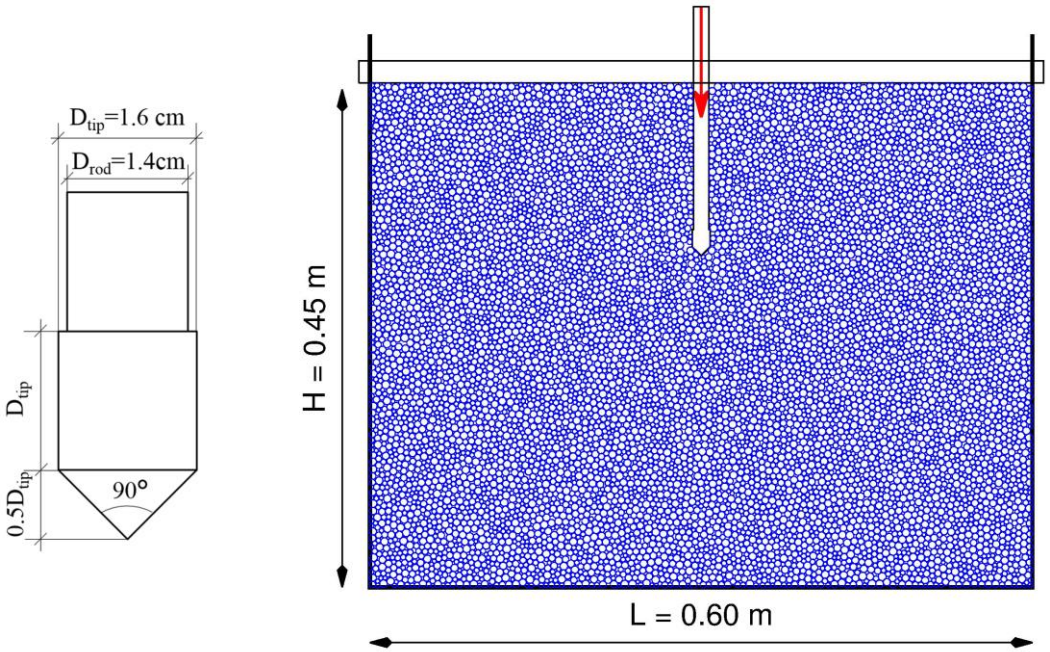

Figure 4. Tip details and sample of granular material tested.

Figure 5 shows the tip force F_c versus the depth in a given sample of 0.60 m width for depth between 0.15 m and 0.30 m, obtained with a rod velocity of 25 mm.s^{-1}. Despite some oscillations, due to coarse nature of the material, it is found that F_c is relatively steady in

average as the depth increases and is keeping with an experimental constant velocity penetration test. The upper confining stress cancelled the effect of the free surface.

In order to highlight the effect of sample width on the test results, constant velocity penetration tests were conducted in boxes of different width ranging from 0.15 m to 0.90 m. The penetration rate used is equal to 1250 mm.s^{-1}, which represents an average value of penetration rates used in this study (constant velocity and impact conditions). Figure 6 shows the probability distribution of F_c obtained for samples width varying between 0.15 m and 0.90 m. As the box width increases, we observe that the probability distribution of the values of F_c becomes stable when the width is greater than 0.60 m.

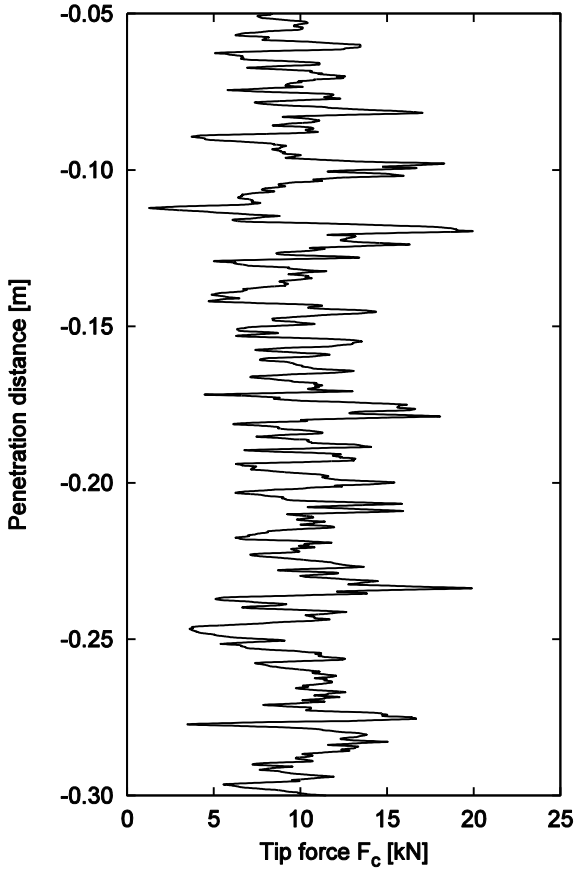

Figure 5. Tip force F_c versus penetration distance obtained at 25 mm.s^{-1} of rod velocity in the sample of 0.6 m width.

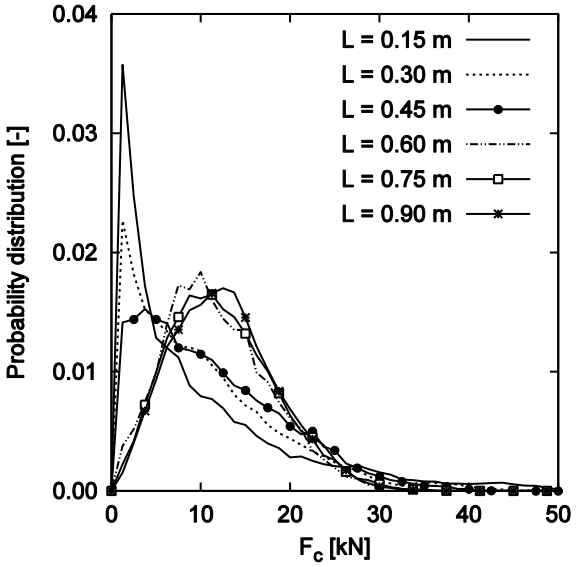

Figure 6. Probability distribution of tip force F_c between 0.05 and 0.30 m of penetration distance at 1250 mm.s^{-1} of rod velocity for different samples width L.

3. Effect of penetration rate on the tip force in constant velocity penetration test

In this section, we focus on the influence of the driving velocity on the tip force F_c for constant velocity penetration tests. The penetration rates range from a low value of, 25 mm.s^{-1} corresponding to penetration rate prescribed in the standards for constant velocity penetration test to a fast penetration rate corresponding to the order of magnitude of impact velocity used in impact conditions 5000 mm.s^{-1} as described in [1,2].

Figure 7 shows the probability distributions of all values of tip force F_c measured between 0.05 m and 0.30 m of penetration depth obtained for three samples with different penetration rates [19]. Probability distributions of tip force F_c complies with the normal law when penetration rate is lower than 1250 mm.s^{-1}. The dispersion of F_c increases when rod velocity is higher than 1250 mm.s $^{-1}$.

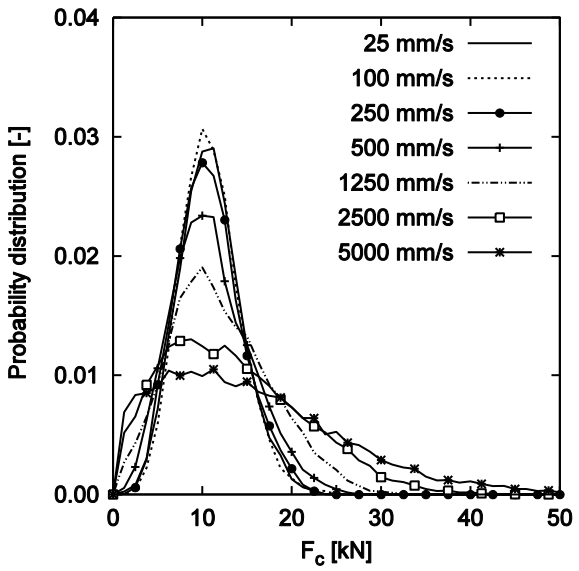

Figure 7. Probability distribution of tip force F_c between 0.05 and 0.30 m of penetration distance for three samples with different rod velocities [19].

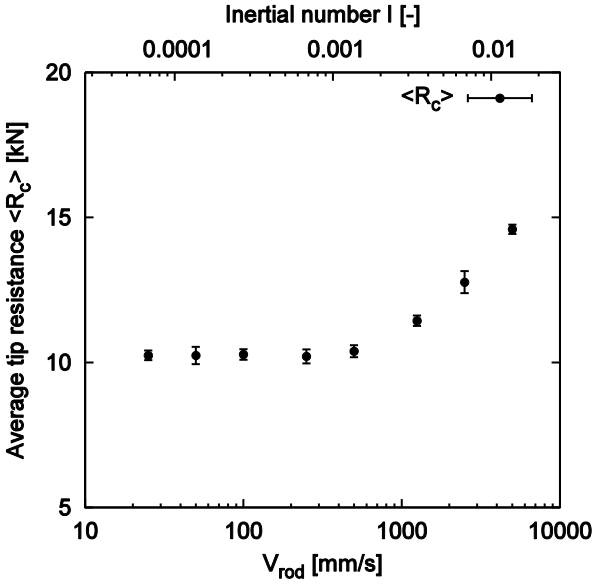

Figure 8. Average tip resistance <R_c> versus rod velocity (height of vertical bars represent twice the standard deviation of R_c).

The non-dimensional inertial number I can be used to quantify dynamic effects in both experimental tests and numerical modeling [17]. Inertial number is given by

$$I = \dot{\gamma}\sqrt{\frac{m}{P}} \tag{1}$$

with $\dot{\gamma}$ the shearing rate of the particle assembly during penetration testing, m the average particle mass and P the confinement stress. It can be used to differentiate the regimes of

solicitation: from quasi–static state with $I < 10^{-3}$ to inertial state with $I > 10^{-3}$ [17]. It is difficult to determine the shearing rate for penetration tests since the deformation applied to the material is highly non-homogeneous. In order to get an order of magnitude of the inertial number, the deformation rate is calculated by the formula being proposed based on V_{rod} the rod velocity; H the sample height:

$$\dot{\gamma} = \frac{V_{rod}}{H} \tag{2}$$

The inertial number I defined by Eq.1 & 2 increases from 6.80×10^{-5} to 1.36×10^{-2} according to the penetration rate (from 25 mm.s^{-1} up to 5000 mm.s^{-1}).

The tip resistance R_c is defined here as the average of F_c obtained between 0.05 and 0.30 m of penetration distance in a given sample. The average tip resistance $<R_c>$ obtained on three different samples is calculated.

It can be observed on Fig.8 that $<R_c>$ remains constant when the rod velocity is lower than 1250 mm.s^{-1}. Then, $<R_c>$ increases increases rapidly for penetration rate upper than 1250 mm.s^{-1} corresponding to an inertial number I (in the order of 3.40×10^{-3}). It can also be noticed on Fig.7 that the dispersion of tip force F_c also increases with rod velocity.

The same trend was described in [4]. In this paper, tip resistance q_c is steady for low value of penetration rates and then increases as penetration rate increases. In both studies, the change of regime occurs for different values of the rod velocity, because this value probably depends on particle size distribution, tip size, confining stress P (as show in Eq.1&2) and possibly additional parameters.

4. Effect of penetration rate on the tip force in impact penetration test

For impact penetration tests, impacts are generated on the top of the driving rod and the tip force F_d is measured as well as the penetration distance.

The effect of impact energy is significant in impact penetration tests. The impact test were compared in terms of maximal rod velocity and not in terms of impact velocity. In order to show that rod maximal velocity is dependent on impact energy, impact tests were conducted with same impact energy but with changing impact mass and impact velocities The ratio between impact mass and rod mass (ξ) for successively taken equal to 0.5, 1.0 and 2.0. Figure

9 presents the three curves of versus penetration distance obtained. First, the magnitude of F_d is similar for 3 cases. Furthermore, the same maximum rod velocity $V_{rodmax} \cong 1210$ mm.s^{-1} is obtained in the different cases corresponding to different ratios ξ (Fig.10).

Secondly, the response obtained with the model is similar to the one classically obtained experimentally (Figure 2), it breaks down into three phases (Fig.9,10):

- a quick loading phase corresponding to the initial increase of the rod velocity. In this phase, whatever is the blow, the signal shape is similar. The duration of this phase is the same as the duration of the impact ($t_{impact} \approx 2.2$ ms). The first point (1) corresponds to the time when the rod velocity reaches its maximum velocity.
- a plastic phase corresponding to the penetration process of the rod in the soil. In this phase, the signal shows oscillations depending on the arrangement of the granular material. The second point (2) corresponds to a moment in this phase when the rod velocity decreases. The point (3) corresponds to the moment when the penetration distance is maximal: the rod velocity is equal to zero.
- a phase of unloading–loading cycles corresponding to the stabilization of the rod. The fourth point (4) shows the moment when the rod velocity is zero for second time.

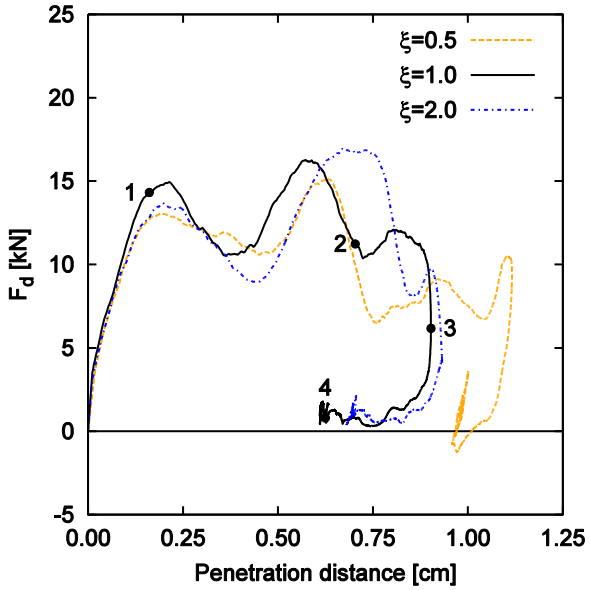

Figure 9. Examples of load–penetration curves obtained for 3 tests performed with the same impact energy.

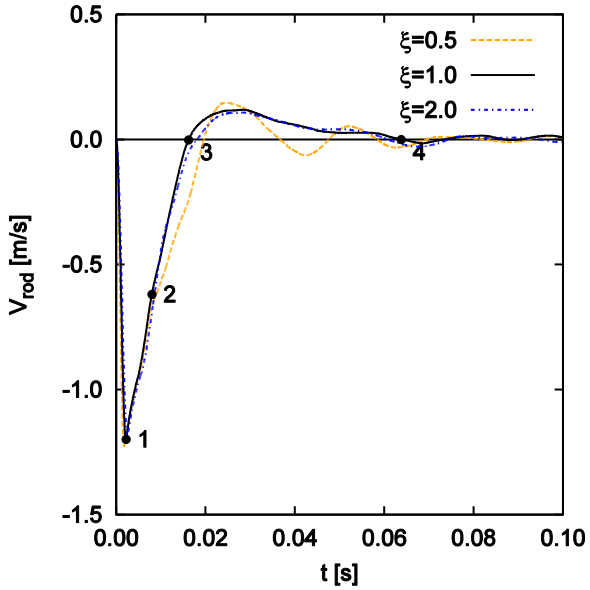

Figure 10. Rod velocity versus time during a impact penetration test for for 3 tests performed with the same impact energy.

Figure 11 shows the load–penetration curve for different impact velocities ($\xi = 1.0$). For an impact velocity of 250 mm/s or smaller, the energy injected is not large enough to drive the rod in the medium: at the end of the impact test, the tip comes back to its initial position; the tip force first increases and then rapidly decreases; the plastic phase of load–penetration curve

(Fig.9) is not observed. For impact velocity of 500 mm.s^{-1} or greater, the tip does not come back completely to its initial position. Figure 11 shows that the minimal velocity required to penetrate the granular material is a value between 250 and 500 mm.s^{-1}. When the impact velocity is greater than 500 mm.s^{-1}, the plateau of the load–penetration curve corresponding to the plastic phase is observed.

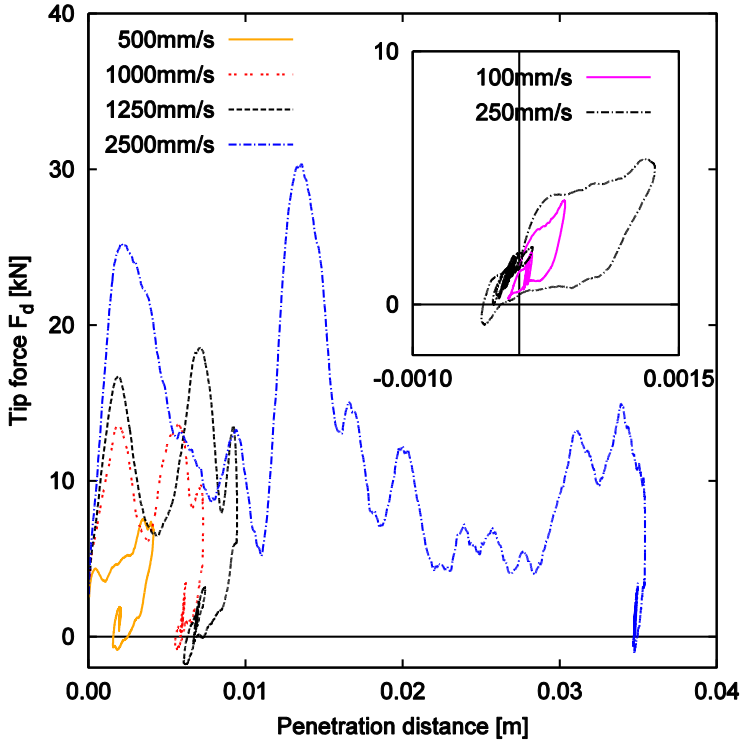

Figure 11. Load versus penetration distance for different impact velocities for impact penetration test.

Although, there is a difference between the maximal penetration distance s_{max} and the final residual penetration distance s_{res} due to the rebound of the rod at the end of the test, the work of the tip force between these two positions is negligible. Consequently, the impact tip resistance R_d of each sample was calculated as the average tip force F_d for penetration distance between 0 and maximal value s_{max}:

$$R_d = \frac{1}{5}\sum_{i=1}^{5}\left\{\frac{1}{s_{max}}\int_{t=0}^{t_{s_{max}}} F_d(t)\,ds(t)\right\}_i \qquad (3)$$

with t the time and t_{smax} the time when penetration distance is maximal and equal to s_{max}.

$\langle R_d \rangle$ is the average value of impact tip resistances obtained on 3 samples. Figure 12 shows the curve of $\langle R_d \rangle$ versus maximal rod velocity V_{rodmax} for different impact energy. We find that $\langle R_d \rangle$ increases when the rod velocity increases.

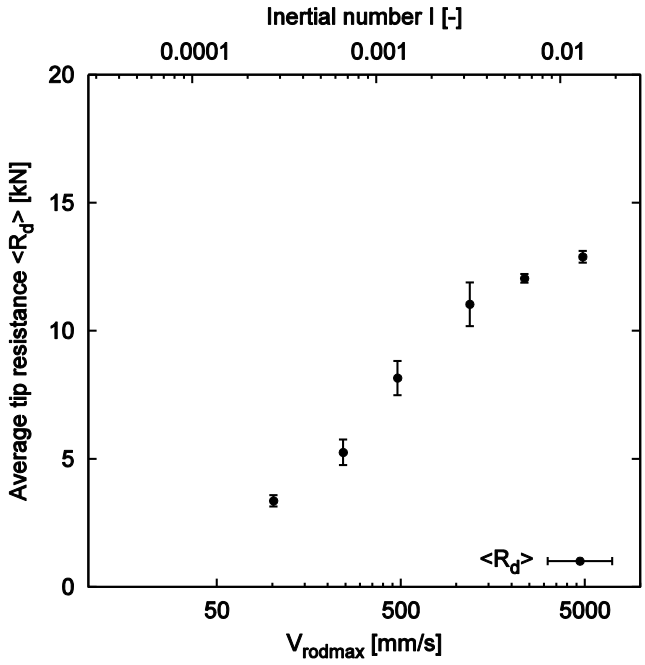

Figure 12. Average tip resistance $<R_d>$ versus maximum rod velocities. Upper x-axis shows the corresponding values of inertial number (height of vertical bars represent twice the standard deviation of R_d).

5. Tip force comparison for constant velocity and impact conditions with different rod velocities

Figure 13 presents the tip force versus penetration distance in both constant velocity and impact conditions for a rod velocity of 500 mm.s^{-1}, corresponding to the quasi–static regime of solicitation. We found that the amplitude of tip force F_d is weaker than the average tip force $<R_c>$. This observation is correlated to the fact that in impact conditions, the impact energy is not sufficient for driving the rod through the granular material. At the end of the phase 1, F_d reaches the value of F_c but then F_d immediately decreases.

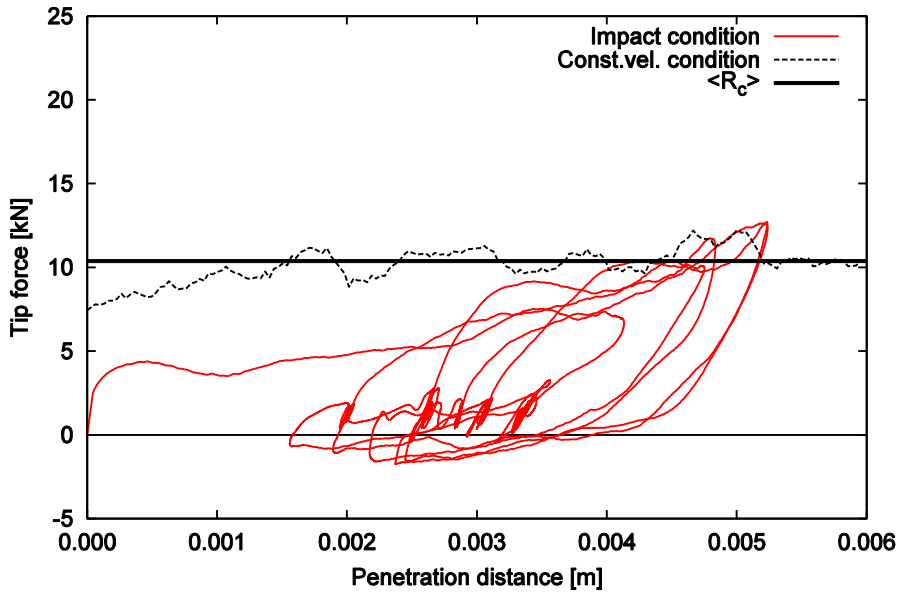

Figure 13. Tip force versus penetration distance for constant velocity penetration test with V_{rod} = 500 mm.s^{-1} and for 5 blows of impact penetration tests performed with V_I = 500 mm.s^{-1}.

Figures 14 and 15 present the tip force versus penetration distance in both constant velocity and impact conditions at 1250 mm.s^{-1} and 2500 mm.s^{-1} of rod velocity range. For this penetration rate, the particle behavior is in the dense flow regime. In contrast to 500 mm.s^{-1} of rod velocity range, we get to generate sufficient energy from the impact to activate the plastic phase. We found that the tip force amplitude is similar in both constant velocity and impact conditions. In addition, the tip force oscillations become more important when the penetration rate increases (Fig.14,15).

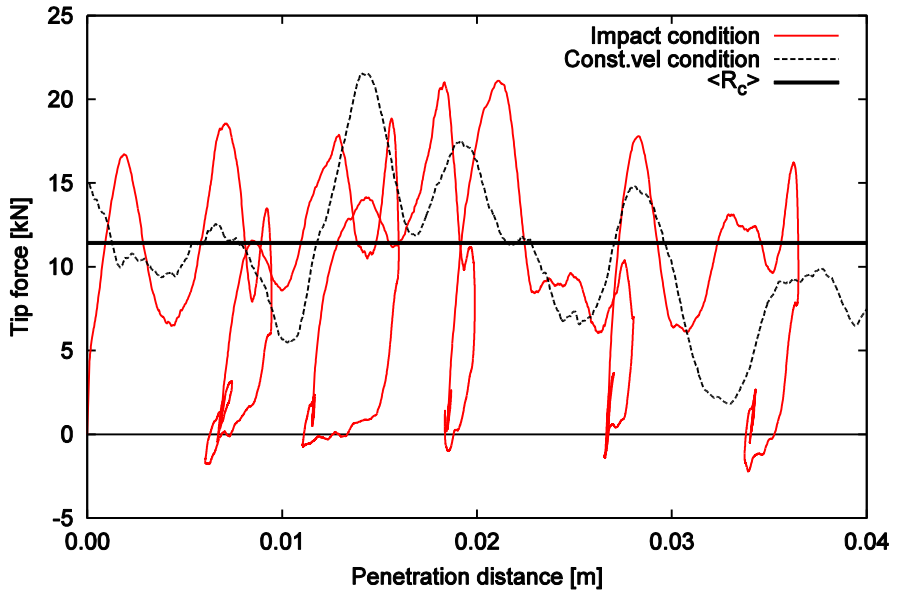

Figure 14. Tip force versus penetration distance for constant velocity penetration test with V_{rod} = 1250 mm.s^{-1} and for 5 blows of impact penetration tests performed with V_I = 1250 mm.s^{-1}.

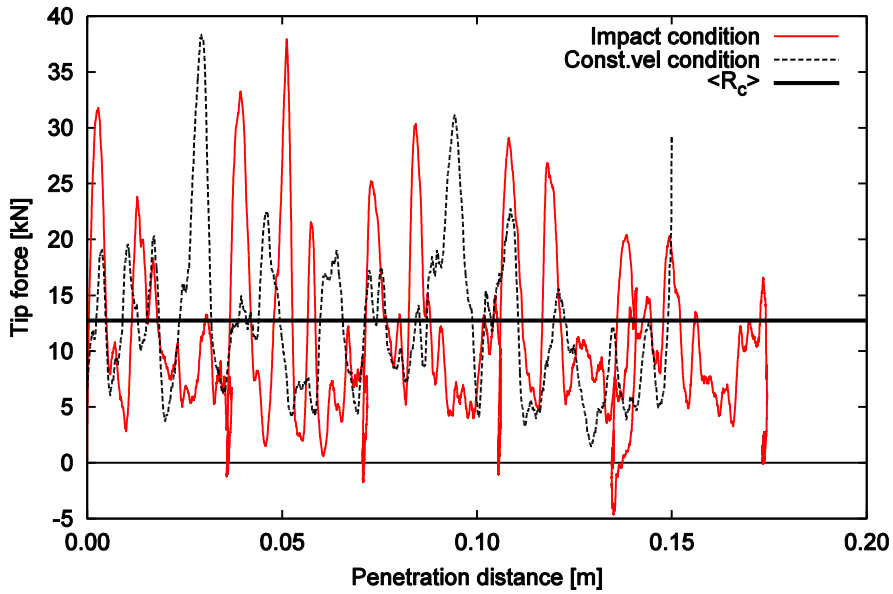

Figure 15. Tip force versus penetration distance for constant velocity penetration test with V_{rod} = 2500 mm.s^{-1} and for 5 blows of impact penetration tests performed with V_I = 2500 mm.s^{-1}.

Figure 16 presents the comparison between the average tip forces obtained in constant velocity and impact conditions at different penetration rates. In fact, the average tip force in a homogeneous medium is stable in the zone where the surface effect is prevented by the vertical confining stress used on top wall. Thus, the average tip force do no depend on the penetration distance for any penetration condition. We note that $<R_d>$ is presented in impact condition as function of maximal rod velocity V_{rodmax}. In quasi–static regime and for similar rod velocity, we found that the $<R_d>$ is smaller than the one obtained in constant velocity penetration test. In dense flow regime ($V_{rod} \geq 1250$ mm.s^{-1}), $<R_d>$ becomes close to $<R_c>$. For high impact energy, the rod velocity in impact condition increases only during the impact. After that, the rod velocity decreases due to the reaction of the particles below the tip. Thus, the $<R_c>$ can be always greater than $<R_d>$ for all rod velocities in dense flow regime.

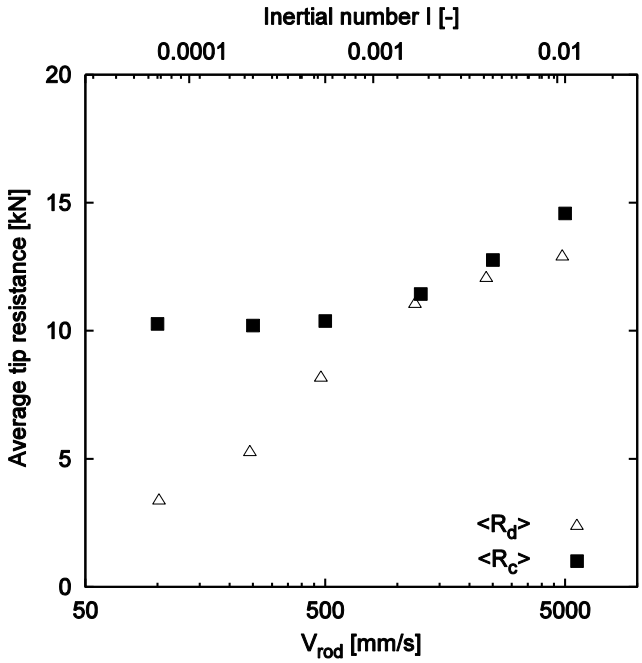

Figure 16. Average tip resistances $<R_c>$ and $<R_d>$ versus rod velocity.

In 3D conditions, we can assume that, as in 2D, an impact energy which is too low can be insufficient to penetrate the material and then to measure a representative tip resistance. On the opposite, for penetration rates high enough, a tip resistance can be measured in impact condition. The increase of tip resistance with the rod velocity was observed in 3D conditions in [4]. In addition, in experimental tests, it is commonly observed that static penetration resistance, measured with low penetration velocity, is lower than dynamic tip resistance, which is measured with relatively high penetration rates. The same trend is observed here on Fig.16: tip resistance in impact condition, for higher rod velocity is greater than tip resistance in constant velocity condition obtained with lower velocity.

6. Conclusion

A 2–dimensional discrete numerical model was proposed to model penetration tests in granular materials. Two types of tests were performed: constant velocity conditions tests and impact conditions tests. The responses obtained in terms of tip forces versus penetration depth is similar to classical experimental results.

Penetration test in soils actually is a three–dimensional problem but was simulated here in plane strain or two dimensions in this study. It is true that an assembly of disks cannot capture exactly the behavior of a real granular material. However, the study presented here focuses only on the mechanisms involved in two different types of penetration tests and on the effect of driving velocity. The study presented here has no intention to link directly and

quantitatively the results obtained in 2D with 3D modelling or field penetration tests. Yet, the basic laws governing the behavior of a mechanical system such as assemblies of disks or spheres are supposed to be shared between those different kinds of systems. Indeed, number of studies proved 2D DEM to be efficient in describing soil behavior [10]. Also, the basic trends observed here are in agreement with other papers focused on 3D simulations.

The effect of penetration rate on constant velocity and impact penetration tests where investigated. The particle behavior changes from quasi–static regime to dense flow regime when rod velocity range varies from 25 $mm.s^{-1}$ to 5000 $mm.s^{-1}$ with a transition value around 1250 $mm.s^{-1}$.

In constant velocity condition, the tip force is stable when the rod velocity is lower than 1250 $mm.s^{-1}$. However, the average tip resistance and the dispersion of tip force increase rapidly when the particle behavior in dense flow regime for a tip velocity greater than 1250 $mm.s^{-1}$.

In impact condition, the load–penetration curves consists in 3 different phrases. The variation of tip force increases in terms of amplitude when the impact velocity increases. In addition, the energy injected is not large enough to drive the rod in the medium in impact condition when the impact velocity is lower than 500 $mm.s^{-1}$.

Finally, the tip forces obtained from impact and constant velocity penetration tests were compared. In quasi–static regime corresponding to impact velocities less than 500 $mm.s^{-1}$, the impact energy is not sufficient for driving the rod through the granular material. For greater impact energy, the amplitude of tip force is closer to but lower than average tip resistance $<R_c>$ obtained in constant velocity test with the same rod velocity. When comparing constant velocity and impact tests, the rod velocity in impact test is the same as in the constant velocity test only at the beginning of the penetration process; as the tip penetrates the material, its velocity progressively decreases and the resulting tip force is lower.

In future tests, it would be interesting to quantify the influence on the results of the contact model and also consider the effect of particle crushing in order to refine the analysis of the results.

Reference

[1] Benz Navarrete, M. (2009). *Mesures dynamiques lors du battage du pénétromètre Panda 2*. PhD thesis, Clermont-Ferrand: Université Blaise Pascal.

[2] Benz, M.A., Escobar, E., Gourvès, R., Haddani, Y., Breul, P. & Bacconnet, C. (2013). Dynamic measurements of the penetration test - Determination of the tip's dynamic load-penetration curve. *Proc. of the 18th Int. Conf. on the Soil Mech. and Geotech. Eng., Paris*, 499 – 502.

[3] Breul, P., Benz, M., Gourvès, R., & Saussine, G. (2009, June). Penetration Test Modelling in a Coarse Granular Medium. In *Powders and Grains 2009: Proceedings of the 6th International Conference on Micromechanics of Granular Media* (Vol. 1145, No. 1, pp. 173 - 176). AIP Publishing.

[4] Quezada, J. C., Breul, P., Saussine, G., & Radjai, F. (2014). Penetration test in coarse granular material using Contact Dynamics Method. Computers and Geotechnics, 55, 248–253.

[5] Huang, A. B. & Ma, M. Y. (1994). An analytical study of cone penetration test in granular material. *Canadian Geotechnical Journal* 31, No.1, 91 – 103.

[6] Huang, A. B. & Hsu, H. H. (2004). Advanced calibration chambers for cone penetration testing in cohesionless soils. *ISC-2 Geotech. and Geophys. Site Characterization, Porto*, 147 – 166.

[7] Calvetti, F. & Nova, R. (2005). Micro-macro relationships from DEM simulated element and in-situ tests. *Proc. 5th Int. Conf. Micromech. Granular Media: Powders and Grains 2005, Stuttgart*, 245 – 250.

[8] Jiang, M. J., Yu, H.-S. & Harris, D. (2006). Discrete element modeling of deep penetration in granular soils. *International Journal for Numerical and Analytical Methods in Geomechanics* 30, No. 4, 335 – 361.

[9] Jiang, M. J., Harris, D., & Zhu, H. (2007). Future continuum models for granular materials in penetration analyses. *Granular Matter*, 9(1), 97–108.

[10] Jiang, M., Dai, Y., Cui, L., Shen, Z., & Wang, X. (2014). Investigating mechanism of inclined CPT in granular ground using DEM. *Granular Matter*, *16*(5), 785-796.

[11] Arroyo, M., Butlanska, J., Gens, A., Calvetti, F. & Jamiolkowski, M. (2011). Cone penetration tests in a virtual calibration chamber. *Géotechnique* 61, No. 6, 525 – 531.

316 [12] McDowell, G. R., Falagush, O. & Yu, H. S. (2012). A particle refinement method for
317 simulating DEM of cone penetration testing in granular materials. *Géotechnique Letters* 2,
318 141 – 147.

319 [13] Robertson, P. K., & Campanella, R. G. (1983). Interpretation of cone penetration
320 tests. Part I: Sand. *Canadian Geotechnical Journal*, 20(4), 718-733.

321 [14] Chaigneau, L. (2001). *Caractérisation des milieux granulaires de surface à l'aide d'un*
322 *pénétromètre*. PhD thesis. Clermont-Ferrand: Université Blaise Pascal.

323 [15] Cundall P. A. & Strack O. D. L. (1979). A discrete numerical model for granular
324 assemblies. *Géotechnique* 29, No. 1, 47 – 65.

325 [16] Combe G. (2002) Mécanique des matériaux granulaires et origines microscopiques de
326 la déformation. *Etudes et Recherches du Laboratoire Central des Ponts et Chaussées*, SI8.

327 [17] Roux, J.-N., & Chevoir, F. (2005). Discrete numerical simulation and the mechanical
328 behavior of granular materials. *Bulletin Des Laboratoires Des Ponts et Chaussées*, (254),
329 109 – 138.

330 [18] Cundall P.A., Drescher A. & Strack O.D.L. (1982). Numerical experiments on
331 granular assemblies: measurements and observations. *IUTAM Conf. on Deformation and*
332 *Failure of Granular Materials, Delft*, 355 - 370.

333 [19] Tran, Q. A., Chevalier, B., & Breul, P. (2015). A numerical study of the penetration
334 test at constant rod velocity. *Computer Methods and Recent Advances in Geomechanics –*
335 *Oka, Murakami, Uzuoka & Kimoto (Eds.)*, p. 193-198.